Two-directional beam-tracking for phase-sensitive x-ray tomography with laboratory sources

Carlos Navarrete-León ✉ ; Adam Doherty; Alberto Astolfo; Charlotte K. Hagen; Peter Munro; Alessandro Olivo; Marco Endrizzi

Check for updates

CrossMark

View Online

Export Citation

Two-Directional Beam-Tracking for Phase-Sensitive X-ray Tomography with Laboratory Sources

Carlos Navarrete-León,[a)] Adam Doherty, Alberto Astolfo, Charlotte K. Hagen, Peter Munro, Alessandro Olivo, and Marco Endrizzi

Department of Medical Physics and Biomedical Engineering. University College London, Malet Place, Gower Street, WC1E 6BT London, United Kingdom

[a)]*Corresponding author: carlos.leon.17@ucl.ac.uk*

Abstract. X-ray phase-contrast imaging is a powerful imaging modality for non-destructive visualisation of weakly-absorbing materials inside an object. We present here a two-directional beam-tracking approach for phase-contrast imaging in a laboratory setup. A single absorption mask is used to modulate the polychromatic x-ray beam, and the divergence of the beam is exploited to analyse the beamlets with detector pixels comparable in size to the mask pitch. The method gives access to two orthogonal phase gradients, which allows for robust phase integration. Two implementations are demonstrated: one with a low-noise photon-counting device for radiography, and the other with an indirect conversion flat-panel detector for phase-contrast tomography. Finally, images of biological specimens are presented to show the potential of the approach for biomedical applications.

INTRODUCTION

Phase-sensitive x-ray imaging is a well-established technique for the non-destructive visualisation of low-Z materials, such as soft tissue in biomedical specimens. It exploits differences in the complex refractive index: $n = 1 - \delta + i\beta$. The real term δ is responsible for the phase shift suffered by the wave field and the imaginary term β is related to the absorption properties of the sample [1]. Using the phase in addition to the absorption signal has two main advantages: an increased contrast for weakly absorbing samples and a slower decrease of contrast as a function of x-ray energy [2].

Different methods have been developed to make use of this principle. Although originally restricted to synchrotron facilities, extensive efforts have been made to adapt interferometric [3] and non-interferometric [4] approaches to laboratory x-ray sources. Such translation has been extended to tomography [5, 6], allowing multi-contrast volumetric representations of the internal structure of an object. These methods make use of a series of phase or attenuation gratings with one-dimensional sensitivity to refraction. Although two-dimensional sensitive adaptations were shown in the lab [7, 8], they still require the acquisition of several exposures while mechanically moving the gratings to quantitatively separate phase and absorption. More recently, the use of a random-phase modulator to create a near-field speckle pattern has drawn attention, due to its simplified set-up as well as single-shot multi-contrast capability [9, 10, 11]. However, due to its relatively high coherence requirements, the method has only been shown with specialised x-ray sources and long propagation distance for tomography [12].

The use of a single absorption mask, an x-ray implementation of the Hartmann wavefront sensor [13], is a suitable candidate for the translation towards laboratory systems, mainly thanks to its extremely low, if not negligible, requirements in terms of spatial and temporal coherence [14]. If the modulator is a 2D structure [15], the method also allows for attenuation, differential phase-contrast, and omni-directional scattering in a single-shot [16, 17]. We present here a two-directional beam-tracking approach for phase-contrast radiography and tomography with a laboratory source. It uses a single two-dimensional absorption mask, placed before the sample, and gives access to two orthogonal differential phase-contrast images for robust phase integration. We demonstrate the method with a low-noise photon-counting device in radiography and an indirect conversion flat-panel detector in tomography. Biological specimens are also investigated as an example of potential applications of the proposed imaging methodology.

MATERIALS AND METHODS

A schematic of the x-ray set-up is presented in Figure 1. It features a Hamamatsu microfocus source (L12161-07) with a W-target used at 40 kVp and 10 W, with a nominal focal spot of 7 μm. The method has been initially tested in two different configurations: with a 100 μm pitch mask and a photon-counting detector for high-sensitivity radiography; and with a 50 μm pitch mask and an indirect conversion flat-panel detector for larger field-of-view tomography.
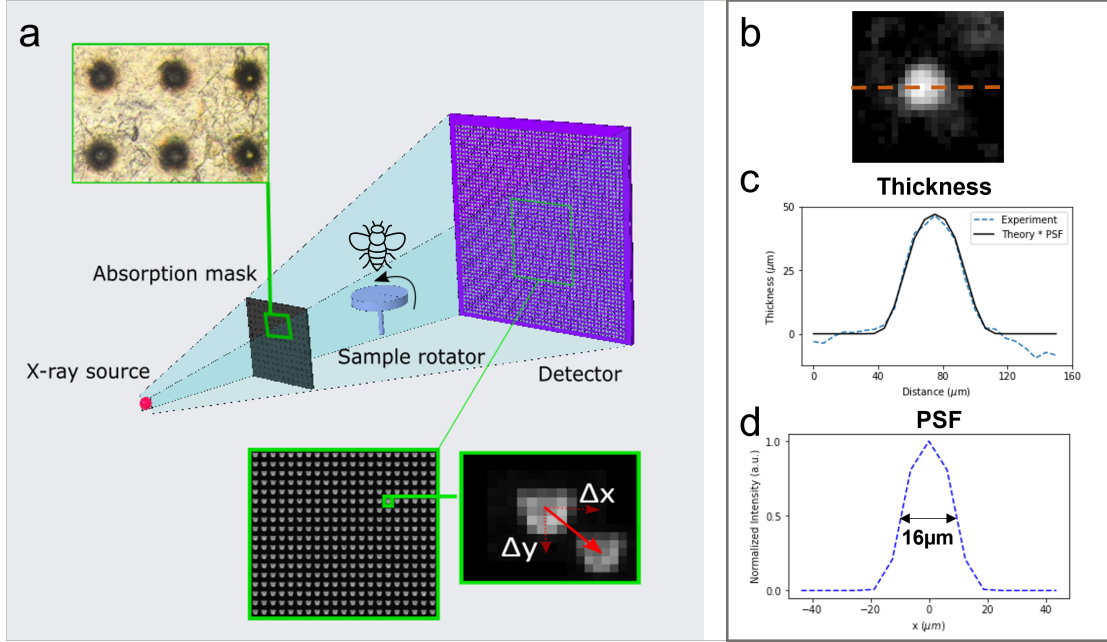
FIGURE 1. Schematic and working principle of the two-directional beam-tracking set-up (a). An experimental image of a 50μm soda-lime glass micro-sphere (b) was used to assess the resolution of the system by matching the theoretical and experimental profiles (c) with a Point Spread Function with FWHM of 16μm (d).

The absorption masks are made with laser-ablation and from readily available 100 μm thick Tungsten foil, and their apertures have conical shape with diameters of ∼15 μm. The photon-counter is a Pixirad-2/PIXIE-III detector with a 62 μm pixel pitch, 650 μm CdTe sensor and 50×32 mm active area. The flat panel is a Hamamatsu detector (C9732DK-11) with a 50 μm pixel pitch, indirect conversion from a CsI scintillator, CMOS sensor and 120×120 mm^2 active area. The source-to-mask (z_{sm}), mask-to-object (z_{mo}) and object-to-detector (z_{od}) distances for the Pixirad configuration are $z_{sm} = 150$ mm, $z_{mo} = 30$ mm and $z_{od} = 680$ mm. And for the flat-panel set-up, these are $z_{sm} = 120$ mm, $z_{mo} = 30$ mm and $z_{od} = 550$ mm.

The absorption mask shapes the x-ray beam into a series of beamlets. The divergence of the x-ray beam magnifies the beamlets, which allows their analysis with detector pixel sizes comparable to the mask pitch. The two-dimensional spatial intensity distribution of the beamlets is analysed independently on a beamlet-by-beamlet basis. When a sample is in the beam, the transmission (t) and the sample induced displacements (Δx and Δy) can be retrieved by comparing the intensity distributions with ($I_s(x,y)$) and without ($I_0(x,y)$) the sample. The transmission is calculated as $t = I_s(x,y)/I_0(x,y)$ and the two displacement vectors are retrieved by registering the two intensity distributions using a sub-pixel cross-correlation algorithm [18].

The orthogonal beam displacements on the detector plane are related to the refraction angles by:

$$\alpha_x(x,y) = \tan^{-1}\left(\frac{\Delta x}{z_{od}}\right) \;, \; \alpha_y(x,y) = \tan^{-1}\left(\frac{\Delta y}{z_{od}}\right) \tag{1}$$

which are proportional to the first derivative of the phase shift ($\alpha_{x,y}(x,y) = \dot{\Phi}_{x,y}(x,y)/k$) and allow using the Fourier derivative theorem to obtain the wavefront profile $\Phi(x,y)$ [7]:

$$\Phi(x,y) = \mathscr{F}^{-1}\left[\frac{\mathscr{F}[\dot{\Phi}_x + i\dot{\Phi}_y](k,l)}{2\pi i(k+il)}\right](x,y) \tag{2}$$

with (k,l) the reciprocal space coordinates to (x, y). This integration approach from two orthogonal phase gradients is more robust and artifact-free compared to numerical integration from 1D gradients, which is advantageous for tomography.

One of the properties of using an absorption mask to redefine the x-ray beam is that the system's resolution is ultimately limited by the mask aperture size [19]. This resolution level can be achieved by mechanically scanning the mask (or the sample) in a 2D grid and stitching the images in a single highly-sampled image. To demonstrate this principle, we imaged a 50 μm soda-lime glass micro-sphere in a 2D grid of 16×16 steps of 7.5 μm and we convoluted the theoretical phase profile with a Gaussian function until it matched the experimental profile (see Figures 1b-d). Following this, we aimed to obtain a resolution close to the mask aperture in our acquisitions. In radiography, a bumble bee was imaged by scanning the sample in a 2D grid of 8×8 steps of 15 μm, to account for the magnification of the mask pitch at the sample plane. The exposure time per step was 1s. For demonstration in tomography, we imaged a carpal joint of a chicken wing; a similar resolution was obtained in this case by scanning the 50 μm pitch mask in a 4×4 sampling grid with 12.5 μm steps for each projection. A total of 2000 projections over 360° were acquired with 1.2 s exposure time, giving a total exposure time of $2000 \times 4 \times 4 \times 1.2$ s = 10.7 h and total acquisition time of 64 h. The rather long acquisition times are due to far-from-optimal synchronisation between positioners and detectors, which we did not optimise for these first tests. The attenuation coefficient μ and the real part of the refractive index δ are reconstructed using the FDK algorithm for cone-beam reconstruction in CUDA, implemented by the Astra Toolbox [20].

RESULTS

The spatial resolution of the system was assessed by matching the measured phase profile of a known object (50um diameter sphere, Fig. 1 b) with the convolution between the point-projected thickness of the sphere and a Gaussian function. The width of the Gaussian function was iteratively changed until the best match (point of minimum residual) was found for FWHM of 16 um. This width is very close to the actual width of the apertures in the modulator. In Figure 2, the refraction in x, refraction in y, integrated phase shift and transmission images are shown for two different regions of the bumble bee. The head and the abdomen of the specimen are shown, where various tissue interfaces and faint details like the wings, antennae, and hair can be observed. By comparing phase and absorption images, an enhanced visualisation of the complex tissue structures in the head and the different tergum segments in the abdomen is realised when using the phase, as indicated by the arrows in the images. In addition, the hairs in the abdomen, the wings coming from the thorax and the anatomy of the legs become visible as a result of the phase-sensitivity of the system. These are further demonstrated in the intensity profiles along the front leg and the wings of the specimen, also presented in the figure, in which the gain in SNR of phase in comparison with transmission is evident.
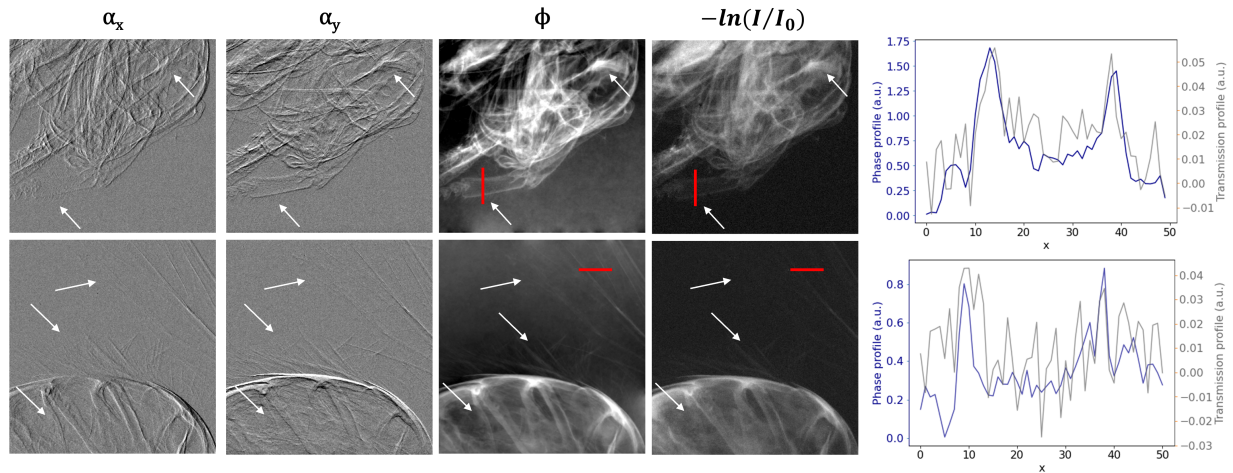

FIGURE 2. From left to right, retrieved images of the refraction along x, refraction along y, integrated phase and transmission of a section of the head (top) and the abdomen (bottom) of a bumble bee. The arrows indicate details visible with enhanced contrast due to the phase-sensitivity as shown by the line plots along the red lines reported in the two boxes on the right hand side.

The axial, longitudinal and coronal slices of the reconstructed phase volume of the chicken wing carpal joint are presented in Figure 3. The spatial resolution is isotropic, i.e. it is preserved across the three orthogonal views
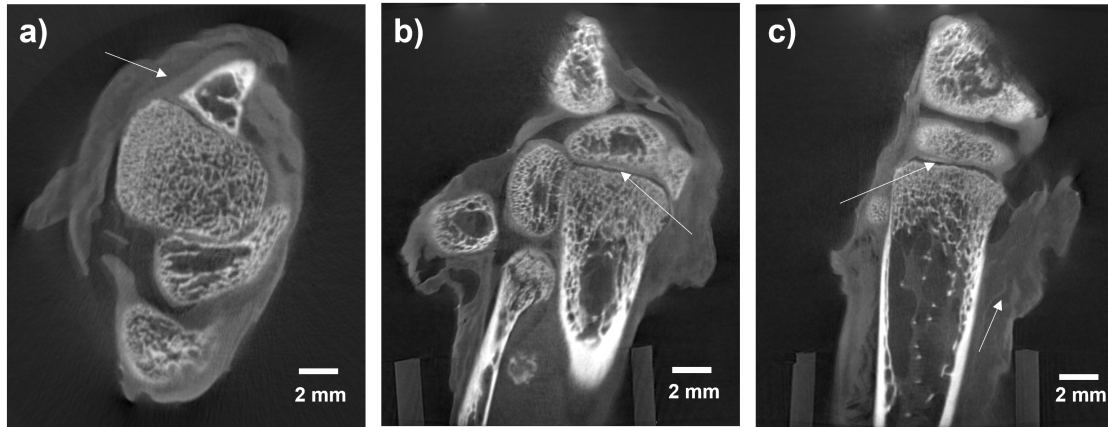
FIGURE 3. X-ray phase-contrast tomography of a chicken wing's carpal joint. Axial (a), longitudinal (b) and coronal (c) slices of the reconstructed volume of the real part of the refractive index (δ) are shown. The arrows indicate regions of soft-tissue contrast.

of the three-dimensional images produced by the system. With phase-contrast tomography, it is possible to obtain simultaneous bone and soft-tissue contrast with high-resolution. Across all slices, the cortical bone and the microstructure of the trabecular bone can be observed in detail. Furthermore, different areas with soft-tissue contrast are also shown by the arrows in the images, including articular cartilage.

CONCLUSIONS

We presented a two-dimensional beam-tracking approach for phase-contrast imaging in a compact laboratory set-up. The system's working principle and data analysis workflow were described, and volumetric reconstructions of the real part of the refractive index (δ) shown. Whilst a complete and quantitative characterisation of the system is underway, images of biological specimens were shown as an indication of the potential for applications in the imaging of weakly-absorbing materials.

ACKNOWLEDGMENTS

REFERENCES

1. D. Paganin, *Coherent X-Ray Optics* (Oxford University Press, 2006).
2. A. Bravin, P. Coan, and P. Suortti, "X-ray phase-contrast imaging: from pre-clinical applications towards clinics," Physics in Medicine & Biology **58**, R1 (2012).
3. F. Pfeiffer, T. Weitkamp, O. Bunk, and C. David, "Phase retrieval and differential phase-contrast imaging with low-brilliance x-ray sources," Nature Physics **2**, 258–261 (2006).
4. A. Olivo and R. Speller, "A coded-aperture technique allowing x-ray phase contrast imaging with conventional sources," Applied Physics Letters **91**, 074106 (2007), https://doi.org/10.1063/1.2772193.
5. F. Pfeiffer, C. Kottler, O. Bunk, and C. David, "Hard x-ray phase tomography with low-brilliance sources," Phys. Rev. Lett. **98**, 108105 (2007).
6. C. K. Hagen, P. R. Munro, M. Endrizzi, P. C. Diemoz, and A. Olivo, "Low-dose phase contrast tomography with conventional x-ray sources," Medical Physics **41**, 070701 (2014).

7. C. Kottler, C. David, F. Pfeiffer, and O. Bunk, "A two-directional approach for grating based differential phase contrast imaging using hard x-rays," Opt. Express **15**, 1175–1181 (2007).

8. G. K. Kallon, M. Wesolowski, F. A. Vittoria, M. Endrizzi, D. Basta, T. P. Millard, P. C. Diemoz, and A. Olivo, "A laboratory based edge-illumination x-ray phase-contrast imaging setup with two-directional sensitivity," Applied Physics Letters **107**, 204105 (2015), https://doi.org/10.1063/1.4935983.

9. S. Berujon, H. Wang, and K. Sawhney, "X-ray multimodal imaging using a random-phase object," Phys. Rev. A **86**, 063813 (2012).

10. K. S. Morgan, D. M. Paganin, and K. K. W. Siu, "X-ray phase imaging with a paper analyzer," Applied Physics Letters **100**, 124102 (2012), https://doi.org/10.1063/1.3694918.

11. I. Zanette, T. Zhou, A. Burvall, U. Lundström, D. H. Larsson, M. Zdora, P. Thibault, F. Pfeiffer, and H. M. Hertz, "Speckle-based x-ray phase-contrast and dark-field imaging with a laboratory source," Physical Review Letters **112**, 253903 (2014).

12. I. Zanette, M. C. Zdora, T. Zhou, A. Burvall, D. H. Larsson, P. Thibault, H. M. Hertz, and F. Pfeiffer, "X-ray microtomography using correlation of near-field speckles for material characterization," Proceedings of the National Academy of Sciences of the United States of America **112**, 12569–12573 (2015).

13. J. Hartmann, "Bemerkungen uber den bau und die justirung von spektrographen," Zt. Instrumentenkd **20**, 47 (1900).

14. F. A. Vittoria, G. K. N. Kallon, D. Basta, P. C. Diemoz, I. K. Robinson, A. Olivo, and M. Endrizzi, "Beam tracking approach for single–shot retrieval of absorption, refraction, and dark–field signals with laboratory x–ray sources," Applied Physics Letters **106**, 224102 (2015), https://doi.org/10.1063/1.4922189.

15. K. S. Morgan, D. M. Paganin, and K. K. W. Siu, "Quantitative single-exposure x-ray phase contrast imaging using a single attenuation grid," Optics Express **19**, 19781 (2011).

16. M. Zakharova, V. Vlnieska, H. Fornasier, M. Börner, T. dos Santos Rolo, J. Mohr, and D. Kunka, "Development and Characterization of Two-Dimensional Gratings for Single-Shot X-ray Phase-Contrast Imaging," Applied Sciences 2018, Vol. 8, Page 468 **8**, 468 (2018).

17. E. S. Dreier, A. Bergamaschi, G. K. Kallon, R. Brönnimann, U. L. Olsen, A. Olivo, and M. Endrizzi, "Tracking based, high-resolution single-shot multimodal x-ray imaging in the laboratory enabled by the sub-pixel resolution capabilities of the mÖnch detector," Applied Physics Letters **117**, 264101 (2020), https://doi.org/10.1063/5.0027763.

18. J. R. Fienup, M. Guizar-Sicairos, and S. T. Thurman, "Efficient subpixel image registration algorithms," Optics Letters, Vol. 33, Issue 2, pp. 156-158 **33**, 156–158 (2008).

19. C. K. Hagen, F. A. Vittoria, M. Endrizzi, and A. Olivo, "Theoretical framework for spatial resolution in edge-illumination x-ray tomography," Phys. Rev. Applied **10**, 054050 (2018).

20. W. van Aarle, W. J. Palenstijn, J. De Beenhouwer, T. Altantzis, S. Bals, K. J. Batenburg, and J. Sijbers, "The astra toolbox: A platform for advanced algorithm development in electron tomography," Ultramicroscopy **157**, 35–47 (2015).

21. C. Navarrete-Leon, A. Doherty, S. Savvidis, M. F. M. Gerli, G. Piredda, A. Astolfo, S. Cipiccia, D. Bate, C. K. Hagen, A. Olivo, and M. Endrizzi, "X-ray phase-contrast micro tomography of soft tissues using a compact laboratory system with two-directional sensitivity," (2022), arXiv:2212.07963 [physics.ins-det].